Image analysis throught multifractal description

Jacques Lévy Véhel, Jean-Paul Berroir

INRIA

INSTITUT NATIONAL DE RECHERCHE EN INFORMATIQUE ET EN AUTOMATIQUE

Image Analysis Through Multifractal Description

Jacques LEVY-VEHEL
Jean-Paul BERROIR

N° 1942
Juin 1993

PROGRAMME 4

Robotique, image
et
vision

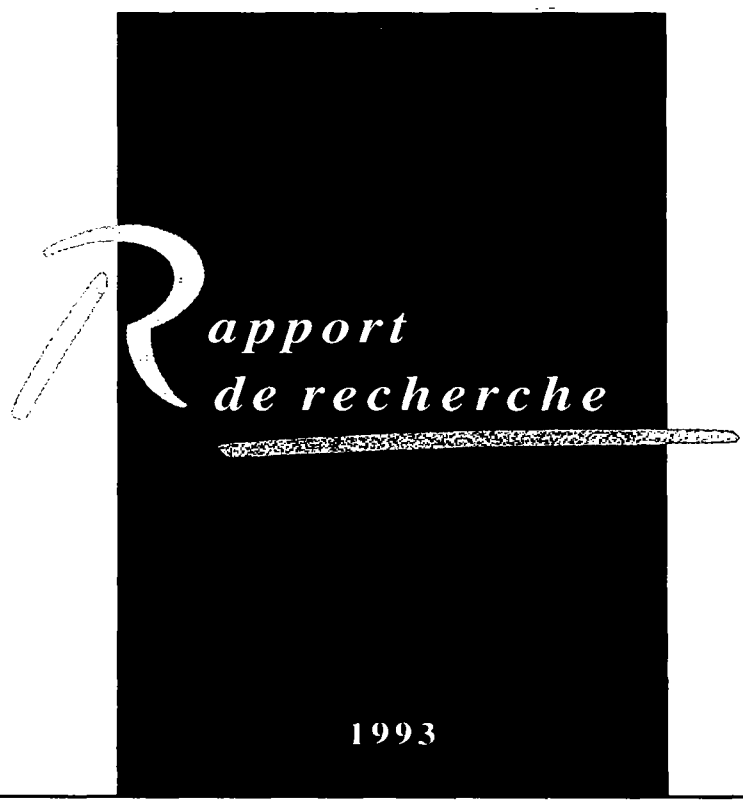

Image Analysis Through Multifractal Description

Description Multifractale de l'Analyse d'Images

Jacques LEVY VEHEL, Jean-Paul BERROIR
INRIA, Rocquencourt
B.P. 105, 78153 Le Chesnay CEDEX, France.
Tel.: +33.(1).39.63.54.73
Fax: +33.(1).39.63.53.30
e-mail: jlv@bora.inria.fr, Jean-Paul.Berroir@inria.fr

abstract

This work is intended to provide a multifractal approach to the problem of edge detection in images.

We show that an alternative description of images, based on the multifractal characterization of the signal, can be used instead of the classical approach that involves smoothing of the discrete data in order to compute derivatives. We focus on the study of edge detection using measures defined as functions of the grey level values in the neighborhood of a given pixel. Each measure is studied through the way it reacts to different types of edges and noise added to the image. Finally, we mention how the use of the multifractal spectrum $(\alpha, f(\alpha))$ may lead to a global approach to the problems of edge detection and region extraction.

Keywords: *image analysis, multifractal, edge detection.*

Résumé

Le but de ce travail est de fournir une approche multifractale au problème de la détection de contours dans une image.

Nous montrons qu'une decription d'images fondée sur la caractérisation multifractale du signal peut être utilisée plutôt que l'approche classique qui suppose le lissage des données discrètes pour calculer des dérivées. Nous nous intéressons à l'étude de la détection de contours en utilisant des mesures définies comme des fonctions des valeurs des niveaux de gris du voisinage du pixel. Chaque mesure est étudiée par sa réaction à différents types de contours et de bruitage de l'image. Enfin, nous montrons comment l'utilisation du spectre multifractal $(\alpha, f(\alpha))$ peut aboutir à une approche globale des problèmes de détection de contours et d'extraction de régions.

Mots-clés : *analyse d'images, multifractales, détection de contours.*

1 Introduction

The aim of this work is to investigate the potentialities of a multifractal approach for image analysis. In the fractal community, "image analysis" usually means that we are given an image representing a certain state of a particular process, and that we want to compute some sort of fractal dimension, which is of interest for characterizing the process, using this image: it can be an aerial photograph of a region showing some faults, in which case we want to evaluate the fractal dimension of the faults network. Another example is electronic micrography of a surface arising in a catalyzed chemical reaction, whose fractal dimension may be related to some parameters of the reaction. Let us also mention the computation of the fractal dimension of a diffusion front from a 2D computer simulation.

Our concern here its totally different: we do not want to use an image representation of a process in order to compute a fractal dimension associated with it, but to characterize the image itself in terms of fractal features.

In other words, the object of study is the image itself, and the fractal approach is used to describe its structure. Thus our work is a fractal approach to the widely studied image analysis problem.

In section 2, we state the basic problems of image analysis and describe some of the "classical" solutions that have been proposed. In section 3, we recall some definitions and results of the multifractal theory. These results are used in section 4 for a multifractal description of images. We present some results on synthetic and real images, before concluding and proposing some desirable extensions.

2 Classical Approach to Image Segmentation

Why do people do Image Analysis?

The answer is because image analysis is the first step for solving the problem of artificial vision, which has many applications in robotics, medical imaging, satellite imaging, etc ...

We restrict ourselves here to the problem of image segmentation: segmentation means that we just want to extract from the image a compact description in terms of edges and/or regions. Thus, we do not tackle the problem of higher level interpretations such as recognition for instance.

Essentially, image segmentation consists in finding all the characteristic entities of an image: these entities are either described by their contours (edge detection) or by the region where they lie (region extraction). These two approaches are dual, but their algorithms are very different, and, unfortunately, most of the times lead to different segmentation results. We shall briefly present some classical methods for these two approaches.

2.1 Edge Detection

It is by far the most widely used approach. The core of the classical methods is the assumption that edges usually corresponds to local extrema of the gradient of the grey levels in the image. The difficulties in edge detection are caused by the noise coming from the camera, the sampling, or the objects themselves.

In this setting, one then has to tackle the problem of computing the derivative of a noisy discrete signal.

Let $I(x, y)$ be the image (noisy) signal. An edge is defined by its type: a step edge is a 0^{th}-order discontinuity of I (see figure 1).

A roof-edge is a 1^{st}-order discontinuity of I (see figure 2).

Other types of contours are defined, but we shall not consider them here (lines, corners, etc ...).

Figure 1: Step edge.

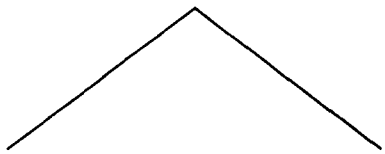

Figure 2: Roof edge.

Let $G(I)$ be the gradient of I.

$$G(I) = \left(\frac{\partial I}{\partial x}, \frac{\partial I}{\partial y}\right)$$

The idea of the approach is to reduce the problem of edge detection to the determination of a filter allowing a good approximation of the gradient G.

Indeed, if we assume that the edge points are local extrema of G, the problem that remains is to accurately compute G.

Under some assumptions on the nature of the noise, it may be shown that the problem is equivalent to that of finding an optimal linear filter f such that:

$$G = (I * f)' = I * f'$$

In order words, we start by smoothing the discrete image data I by convolving it with f, and then compute the gradient by differentiating the smoothed signal. Edge points are then defined to be the local maxima of the gradient's norm in the gradient's direction.

It remain to define some criteria for the performance of the smoothing filter, in order to find an optimal one. Usually the following three criteria are considered:

- Detection: the operator must react to an edge.
- Localization: the edge must be precisely detected.
- One response to one edge: an edge must trigger the operator only once.

Under the assumption that the edge is a step edge and that the noise is additive, white, and gaussian, it may be shown that the optimal filter is (in 1D):

$$f(x) = a_1 e^{\alpha x} \sin(wx) + a_2 e^{\alpha x} \cos(wx) + a_3 e^{-\alpha x} \sin(wx) + a_4 e^{-\alpha x} \cos(wx) + c$$

where α, w and c are real positive constants, and:

$$f(0) = 0, f(W) = 0, f'(0) = S, f'(W) = 0$$

W being the width of the filter (see [7]).

People usually use:

$$f(x) = -ce^{-\alpha|x|} \sin(wx) \quad \text{or} \quad f(x) = -cxe^{-\alpha|x|} \qquad \text{(Canny-Deriche filter)}$$

which corresponds to infinite W (see [8]), or simply a gaussian filter:

$$f(x) = ce^{-\alpha x^2}$$

The parameter α allows to tune the smoothing of the signal, and thus to adjust the trade-off between localization and robustness to noise.

For a more complete description of the classical approaches, see [24].

2.2 Region Extraction

We very briefly state the main points of this approach. The idea here is to separate the image into regions that verify a given uniformity criterion.

If we are dealing with very simple images, the criterion might just be that all points belonging to a certain region must have the same grey level. However, in general, images include textured zones, and one has to solve the much harder problem of texture discrimination. For more complete discussion, see [23], [6].

3 Basics of the Multifractal Theory

We briefly recall some basic facts about the multifractal theory. See also [9], [10], [11], [22], [21], [17].

Let μ be a Borel probability measure on $[0,1] \times [0,1]$. Let ν_n be an increasing sequence of positive integer, and define:

$$I_{i,j,n} = \left[\frac{i}{\nu_n}, \frac{i+1}{\nu_n}\right] \times \left[\frac{j}{\nu_n}, \frac{j+1}{\nu_n}\right]$$

We consider the following quantities:

$$\tau_n(q) = -\frac{1}{\log \nu_n} \log \sum_i{}^* \sum_j{}^* \mu(I_{i,j,n})^q$$

where $\sum^*$ means that the summation runs through those indices (i,j) such that $\mu(I_{i,j,n}) \neq 0$.

We shall say that μ has a multifractal behaviour if:

$$\lim_{n\to\infty} \tau_n(q) = \tau(q)$$

exists for q in a non empty interval of $\mathbb{R}$.

$\tau(q)$ characterizes the global behaviour of the measure when the size of the intervals tends to zero. $\tau(q)$ is related to an notion of generalized dimensions. Indeed, if we define:

$$\begin{aligned} D_q &= \frac{1}{q-1}\tau(q) \qquad q \neq 1 \\ D_1 &= \lim_{q\to 1}\left[\frac{1}{q-1}\tau(q)\right] \end{aligned}$$

then D_0 is the fractal dimension of the support of μ, D_1 is the information dimension, D_2 the correlation dimension, etc ...

Set:

$$I_n(x,y) = \{I_{i,j,n} / (x,y) \in I_{i,j,n}\}$$

We define:

$$E_\alpha = \left\{(x,y) \in [0,1[\times[0,1[/ \lim_{n\to\infty} \frac{\log \mu(I_n(x,y))}{\log \nu_n} = -\alpha\right\}$$

The exponents α characterize the local scaling behaviour of the measure: if α exists at point (x, y) then we have:

$$\mu(I_n(x, y)) \sim (\nu_n)^{-\alpha(x,y)} \text{ when } n \to \infty$$

ν_n being the linear size of the "box" around (x, y) upon which we evaluate μ. α is called the Hölder exponent at point (x, y).

E_α can then be seen as the subset of points having the same scaling behaviour, described by α.

To have a multifractal description of μ, one first compute the set of possible α exponents, and then evaluate the "size" of the subset E_α of $[0, 1[\times[0, 1[$ associated with α, by computing the Haussdorff dimension of E_α, often denoted by $f(\alpha)$.

This $(\alpha, f(\alpha))$ description is thus both local (via α) and global (via $f(\alpha)$). It is called the multifractal spectrum of μ. Several interpretation of these quantities can be made. One of the most important is the link between $f(\alpha)$ and the rate function appearing in the theory of large deviations. Briefly, this means that the exponential of $(f(\alpha) - D)$ measures the decay of the probability of finding the value α when n tends to infinity, where D is the dimension of the embedding euclidean space.

A central concern in the multifractal theory is to link both descriptions, namely $(\alpha, f(\alpha))$ and $(q, \tau(q))$. This has important applications. Indeed, $\tau(q)$ is usually much easier to compute on experimental data than $(\alpha, f(\alpha))$: $\tau(q)$ is obtained by averaging over many "boxes" and then taking the limit. α is more sensitive to noise, since it is computed independently at each point. As for $f(\alpha)$, it implies the computation of a Haussdorff dimension, which is typically very involved.

Under very general assumptions, it has been proven that (see [6]):

$$f(\alpha) \leq \inf_q(q\alpha - \tau(q))$$

For certain special classes of measures, including multinomial measures, we have an equality:

$$f(\alpha) = \inf_q(q\alpha - \tau(q))$$

That is, the Haussdorff dimension of E_α is obtained through a Legendre transform of $\tau(q)$..

In this case, an analogy with thermodynamics can be made, with the following equivalences:

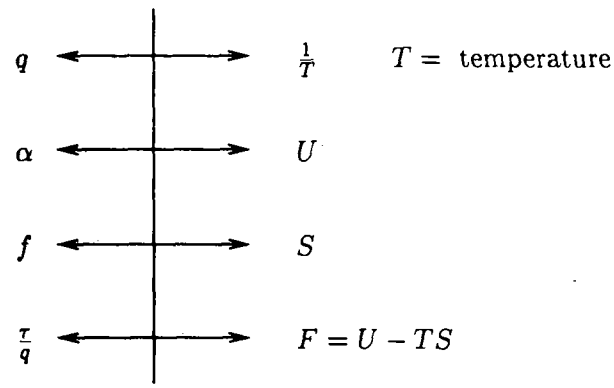

In the case of multinomial measures, $f(\alpha)$ is a bell-shaped curve. This shape is also observed for a number of natural phenomena. However, this is by no way a general property, as one can prove that any ruled function can be the spectrum of a multifractal measure (see [12]).

Other "special" features of f may appear depending on the construction of the measure, as for instance negative values (see [21]).

4 Application to Image Analysis

4.1 Definition of the measures

Though fractal geometry has been introduced a long time ago in image analysis, it is not yet used extensively ([20], [5], [4], [2], [16], [3], [27]).

Some authors have used the fractal dimension to perform texture classification and image segmentation ([26],[27]), other have used higher order dimensions or measures, as correlation or lacunarity ([14],[15]), to refine the results and have obtained some interesting results. Very few papers have been devoted to the use of multifractals in image analysis ([1], [18]), although multifractals are intensively studied in mathematics, physics, meteorology and other fields ([19], [25], [13], [10], [11], [28], [18]).

The main point that justifies the introduction of multifractals in image analysis is the following one:

Fractal dimension is a nice tool for characterizing the irregularity of a curve or a surface. Though its measurement is not very precise on images, it is fast to compute and can sometimes help to get specific features from the data. However, it seems to us that applying it to characterize an image is totally unfounded. This approach assumes that the 2D grey level image can be seen as a 3D surface, or, equivalently, that the grey levels can be assimilated to a spatial coordinate on the z-axis. This assumption has no theoretical basis and we believe that it leads to a fundamentally false analysis of the image, since the scaling properties of the grey levels are totally different from those of the space coordinates. Instead, we should look at the grey levels as a measure, laid upon a generally compact set, totally inhomogeneous to space coordinates. We shall define the measure of a region as a given function of the grey levels of the points of the region.

In this framework, we may now appeal to fractal tools to solve some specific problems. The correspondent of fractal dimension (which is a notion that refers to set) for measures are the multifractal characterizations.

A natural choice is to define the measure μ as the sum of intensities of pixels in the measured region. This definition respects measure's theory axioms, we shall now call it "sum" measure.

We may also generalize the notion of Hölder exponent by introducing definitions of μ that does not necessary respect measure's theory axioms. We introduce "max", "min" and "iso" measures of a region Ω. If $\Omega^\star$ is the subset of Ω where intensity is non-zero, and $p(i)$ is the intensity of the point i, we define:

$$\mu_{\max}(\Omega) = \max_{i\in\Omega} p(i) \tag{1}$$

$$\mu_{\min}(\Omega) = \min_{i\in\Omega^\star} p(i) \tag{2}$$

The iso measure depends on an under discretization of gray levels such that:

$$p^\delta(i) = p^\delta(j) \Longleftrightarrow |p(i) - p(j)| < \delta$$

If $G(\Omega)$ is the geometrical center of Ω, we define:

$$\mu_{\text{iso}}(\Omega) = \text{Card}\{i \in \Omega / p^\delta(i) = p^\delta(G(\Omega))\} \tag{3}$$

We shall see that exponents computed with those measure gives different informations on the singularities encountered: $\alpha_{\max}$ and $\alpha_{\min}$ only depends on the height of the singularity, α_{iso} only depends on the kind of singularity, and α_{sum} depends on both height and kind of the singularity.

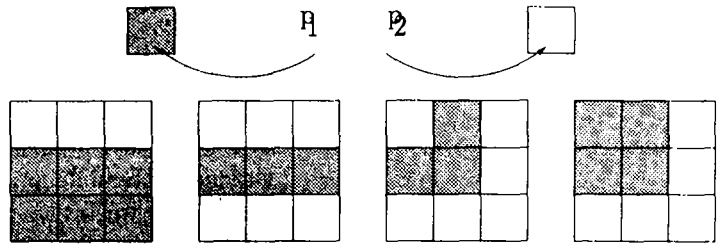

Figure 3: Step-edge, line , corner line and corner models. Notice that the line and the line corner model give the same measure, they won't be distinguished further.

4.2 Edge detection using multifractal characterizations

4.2.1 Introduction

Our approach is, in some sense, inverse to the classical one explained in section 2: instead of smoothing the discrete data in order to be able to compute some derivatives, we stay with our initial discrete values and quantify the singularity around each point; we then characterize an edge point as a point having a given value of singularity.

This procedure is based on the idea that, in some cases, it might be impossible to recover an underlying continuous process from the discrete data (if such a process exists ...). Thus it seems more natural to directly model the sampled signal. The advantage is that we do not loose or introduce any information by smoothing. The drawback is that we may well be much more sensitive to noise. This is why we have to define several measures, and use all the tools of the multifractal theory.

Our segmentation process supposes that multifractal exponents respond to signals such as step-edges, lines, or corner. They bring an information about the local behaviour of measure, more precisely how measure does behave when increasing scale. It is obvious that this comportment is affected by the presence of a singularity.

Canny-Deriche filtering is proved to be optimal among linear filters to a step-edge model with gaussian noise. Step-edge is not the only model available to characterize an edge. A problem often encountered is the detection of edges containing corners or junctions: in this case, gradient isn't meaningful for we cannot approximate the signal by a differentiable function. We also want our edge detector to be idempotent: the result of an edge detection is made out of lines, which are not detected by the Canny-Deriche filter. One has to use a specific filter. We believe that one can ask an edge detector to detect its own result.

In this section, we study how do multifractal exponents behave when a singularity is encountered. "sum", "max", "min" and "iso" measures are studied, we compare the values of the related exponents on three models of singularities (step-edge, corner and line) with the value taken on a plane. Figure 3 describes those singularities. These are simplified models with only two values of gray levels, p_1, level of the point of interest, and p_2, level of the background. We will denote $V(i)$ the $i \times i$ squared neighborhood centered on the pixel of interest, and $V^*(i)$ as $V(i)$ minus the pixel of interest.

α is computed as the estimation of the slope of $\log \mu(V(i))$ versus $\log i$, with $i = 2n+1$, $n = 0 \ldots$. The maximal size of neighborhoods is related to localization of computation. If we use little neighborhoods, for instance $i \leq 3$, α will react to localized singularities, if we use larger neighborhoods, α will react to more widespread singularities. Notice that α only depends on the variation of measure with scale,

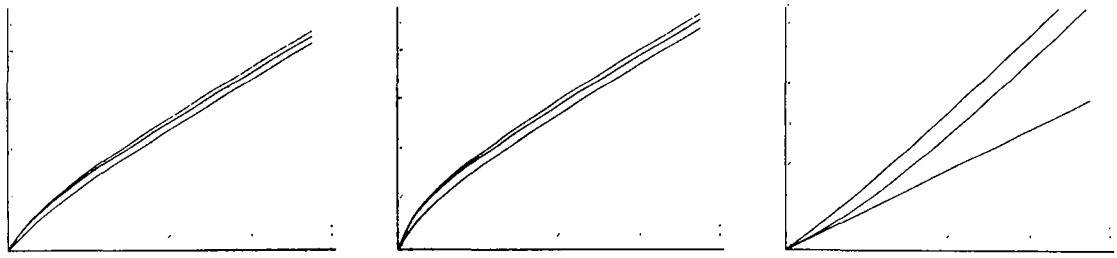

Figure 4: Left: sum measure, from bottom to top, response to a step-edge, a corner and a line with $\lambda = 5$; Middle: sum measure, from bottom to top, response to a step-edge, a corner and a line with $\lambda = 10$; Right: iso measure, from bottom to top, response to a line, a corner and a step-edge. α is estimated as the slope of each of these curves.

regardless of the geometry of the singularity. Hence, we can compute α even in cases where gradient approach fails. The following study is led in 2D.

"sum" measure: We have $\mu(i) = 9p_1$ for a plane, $\mu(i) = (2n+1)(np_2 + (n+1)p_1)$ for a step-edge, $\mu(i) = n(3n+2)p_2 + (n+1)^2 p_1$ for a corner and $\mu(i) = (2n+1)p_1 + (2n+1)(2n)p_2$ for a line. This measure leads to an exponent dependent of the kind of singularity and its relative height $\frac{p_2}{p_1} = \lambda$. For given values of p_1 and p_2, with for instance $p_2 > p_1$, $\alpha = 2$ for a plane, then is bigger for a step-edge, still bigger for a corner and at last is highest for a line.

"max" and "min" measure: We have $\mu(i) = p_1$ for a plane, $\mu(i) = \max(p_1, p_2)$ and $\mu(i) = \min(p_1, p_2)$ for these measures whatever is the singularity. These measures are only significant when using little neighborhood: as for $n > 0$, $\mu(i)$ is constant, large neighborhoods leads to $\alpha = 0$. Using these measures with little neighborhoods induces the same reaction to any kind of singularity.

"iso" measure: We have $\mu(i) = (2n+1)^2$ for a plane. If the singularity height is big enough with respect to the new discretization of gray levels, reaction of α is independent to the height, it only depends on the kind of singularity, We have indeed $\mu(i) = n(2n+1)$ for a step-edge, $(n+1)^2$ for a corner and $2n+1$ for a line. Using this measure enables us to distinguish between different singularities, provided it is higher than a given threshold, regardless of the values of gray levels.

Figure 4 shows the different responses to a step-edge, a corner and a line, for the sum and iso measure, as the plot of of $\log \mu(i)$ vs $\log(i)$. Estimation of the slope of each of theses curves gives the corresponding exponent α, and in general tends to the same limit as the resolution grows. One has to perform a local study to detect singularities, that is no more than 9 pixels of maximal resolution. It is very important to notice that sum measure gives a response depending on the relative height λ of the step-edge, corner or line, and that iso measure gives a response only dependent on the type of singularity.

α provides efficient tools to singularity detection. The choice of the measure depends of what the user wants: "max" or "min" measure can be used with small neighborhoods to detect any singularity. To have a reaction dependent of the height of the singularity (as gradient does), "sum" measure is adapted. At last, "iso" measure enables us to classify the singularities among line, corner, step-edge or no singularity (in this case, $\alpha = D$, where D is the euclidean dimension of the space), provided they are high enough. Notice that reaction to corner and lines, for which a gradient approach is inadapted, leads to higher responses than to step-edges, when using "sum" and "iso" measure.

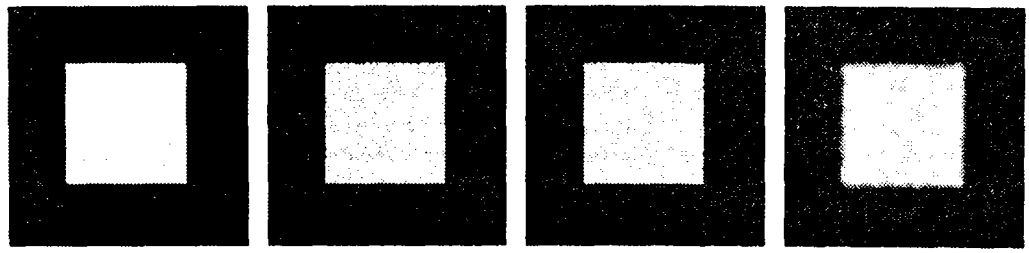

Figure 5: Different kind of blurring, from left to right: original image, gaussian noise, uniform noise, Rayleigh noise.

4.2.2 Study of robustness to noise and blurr

To show that multifractal exponents are useful for edge detection in real situations, we have to study the effect of blurring: depending on the acquisition process, natural images are affected with different types of noise. The most widely used model of noise is the gaussian white noise, that affects the regularity of intensity, but not the shape of objects in the image. The white uniform noise gives the same effect. Those models are not fitted to all modalities of acquisition. Radar or echographic images are affected by correlated noise, that also induces deformation of shapes, leading to fuzzy images. Multiplicative noises, and mostly the Rayleigh multiplicative noise, provide a good model to this. Figure 5 illustrates this, showing the effect of gaussian noise of variance 0.1, uniform noise of amplitude 0.1 and Rayleigh noise of variance 0.1 on a square image.

We have studied the influence of different kinds of noise on our model: gaussian and uniform white noise, and Rayleigh multiplicative noise have been studied on step, line and corner models. Comparison are done with the plane model, that has no singularity.

We have divided this work in two parts: a theoretical approach has been performed in simple cases. When this was not possible, a numerical simulation was applied. In all cases, our aim is to obtain the density function of α considered as a random variable, depending on the kind of model used for the image, the SNR ratio, and of course the exponent computed.

Theoretical approach In some simple cases, one can directly compute the law of α. If we consider a computing neighborhood $V(3)$, the expression of α reduces into (4), where only 2 variables x and y appear: x is the measure of the neighborhood, and y the measure of the pixel itself.

$$\alpha = \frac{\log \mu(V(3)) - \log \mu(V(1))}{\log 3 - \log 1} = \frac{\log \frac{x}{y}}{\log 3} \tag{4}$$

This study has been led in this case, with gaussian and uniform white noise, and the "sum" measure and the "max" measure. All other cases (other measures, Rayleigh noise, larger neighborhood) have been studied by numerical simulation.

The computation of the law divides itself into three steps: Computing the joint law of x and y, given the law of all pixel in $V(3)$; computing the law of $\frac{x}{y}$, x and y being non independent random variables, and computing the law of α.

We shall denote f_{var} the density function of the variable var, and F_{var} the repartition function. x is the measure of $V(3)$, y the measure of the pixel of interest, and t is the measure of $V^{\star}(3)$.

Computing the joint law of x and y In the case of additive white noise, each pixel value in the neighborhood are independent random variables. x and y aren't independent, but this is true for t

and y. The computation of the law of the ratio $\frac{x}{y}$ requires the joint density function f_{xy}. In the case of gaussian noise, there exists a famous expression of it, but not in the case of uniform noise: it will be easier to compute the law of t.

Gaussian noise of variance σ^2, "sum" measure

x is the sum of 9 independent gaussian variable, and so x is a gaussian variable of mean $np_1 + (9-n)p_2$ ($n = 3$ for a line, 6 for a step, and 4 for a corner) and variance $9\sigma^2$. y is a gaussian variable of mean p_1 and variance σ^2. We also have $x = y + t$, $\bar{t} = \bar{x} - p_1$ and $\sigma_t^2 = 8\sigma^2$, y and t are independent variables. The correlation rate r between x and y is $\frac{Cov(x,y)}{\sigma_x \sigma_y}$. It is easy to see that $r = \frac{1}{3}$. The joint law is the law of two gaussian $(np_1 + (9-n)p_2, 9\sigma^2)$ and (p_1, σ^2) of correlation rate $\frac{1}{3}$.

Uniform noise of amplitude T, "sum measure"

The sum of uniform random independent variables converges very quickly to a gaussian variable, we will then approximate the sum of $n \geq 3$ uniform variables with a gaussian of variance $n\frac{T^2}{12}$. t and y being independent and $x = y + t$ leads to the joint law (5):

$$f_{xy}(x,y) = f_y(y) f_t(x-y) \tag{5}$$

where f_t is the density of a gaussian variable of mean $(n-1)p_1 + (8-n)p_2$ and variance $8\frac{T^2}{12}$, f_y being the density of a uniform variable of mean p_1 and amplitude T.

Uniform noise, "max" measure

We now have $x = \max(y,t)$, y and t are independent. We finally obtain the joint density (6):

$$\begin{aligned} x < y &\implies f_{xy}(x,y) = 0 \\ x \geq y &\implies f_{xy}(x,y) = f_y(y) f_t(x) \end{aligned} \tag{6}$$

We suppose that $|p_1 - p_2| > T$, which means that the singularity height is significant. The case $p_1 > p_2$ for the "max" measure is of poor interest, for the step is not detected. If $p_2 > p_1$ we find:

$$\forall t \in [p_2 - \frac{T}{2}, p_2 + \frac{T}{2}], f_t(t) = \frac{1}{T^{9-n}}(t - p_2 + \frac{T}{2})^{8-n}$$

$$\forall t \notin [p_2 - \frac{T}{2}, p_2 + \frac{T}{2}], f_t(t) = 0$$

with $n = 3$ for a line, 6 for a step, and 4 for a corner.

Finding the law of $z = \frac{x}{y}$ Let D_z be the region of the (x,y) plane such that $\frac{x}{y} \leq z$. We find the repartition function by computing the mass of D_z, and by differentiation the density is given by (7).

$$f_z(z) = \int_0^\infty y f_{xy}(zy, y) dy - \int_{-\infty}^0 y f_{xy}(zy, y) dy$$

$$f_z(z) = \int_{-\infty}^\infty |y| f_{xy}(zy, y) dy \tag{7}$$

4.2.3 Law of α

As $\alpha = \frac{\log z}{log 3}$, computation of the repartition function leads to (8):

$$f_\alpha(\alpha) = 3^\alpha \log 3 f_z(3^\alpha) \tag{8}$$

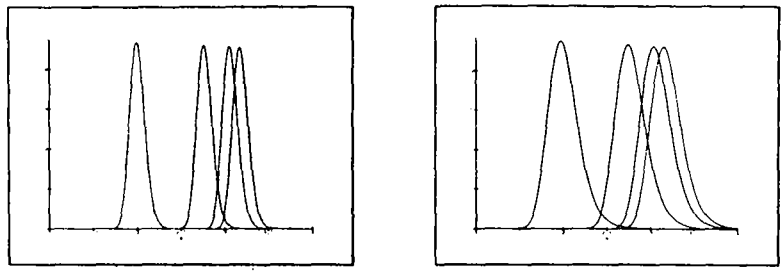

Figure 6: Density of α for gaussian noise; Left: $s_1 = 10$ and $s_2 = 50$, right: $s_1 = 5$ and $s_2 = 25$; On each figure, plots represent from left to right the density for a plane, a step, a corner and a line. Value of α without noise: plane: 2, step: 2.77, corner: 3.07, line: 3.18.

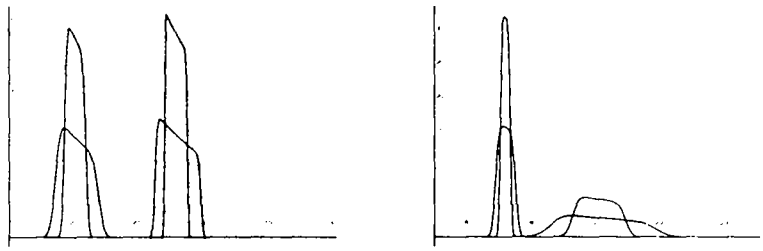

Figure 7: Density of α for sum measure, uniform noise. Left plot shows on the left densities for a plane with $s = 5$ (high peak) and $s = 2.5$ (wide peak), and on the right density for a step, $s_1 = 5$ and $s_2 = 25$ (wide peak), $s_1 = 2.5$ and $s_2 = 12.5$ (large peak). Right plot shows on the left, density for a step, $s_1 = 25$ and $s_2 = 5$ (wide peak), $s_1 = 12.5$ and $s_2 = 2.5$ (high peak) and on the right, density for a plane, $s = 5$ and $s = 2.5$.

Following this process gives the density f_α. Expressions of f_α are rather complex and are not useful for comprehension. We prefer to show different plots of f_α, depending on the variables s_1 and s_2, which are a kind of SNR ratio, with $s_i = \frac{p_i}{\sigma}$ in the case of the gaussian noise, $s_i = \frac{p_i}{T}$ in the case of the uniform noise.

Gaussian noise, sum measure

The law is plotted on figure 6. Observation of plots shows that there is nearly no chance of confusion between a plane and a singularity, even though sum measure isn't an efficient tool to distinguish the different singularities.

Uniform noise, step-edge, sum measure

The law is plotted on figure 7, which also shows the density in the case of a plane. The theoretical value of α on a plane while the sum measure is 2. Observation of the plot shows that the step is always detected, even if the SNR ratio is weak. As an exponent computed using sum measure reacts more strongly to corner and lines than to steps , those singularities cannot be confused with a plane.

We can conclude that the α exponent computed with sum measure is robust to uniform and gaussian noise.

Uniform noise, step-edge, max measure

Computation has been led for $p_2 > p_1 + T$. The integration of joint density leads to the following density plotted on figure 8. We didn't study the distribution for lines or corner, for max measure reacts the same way to them than to steps. We can see that steps (as well lines or corners), even with a weak SNR, are never confused with a plane. "max" measure is also robust to uniform noise.

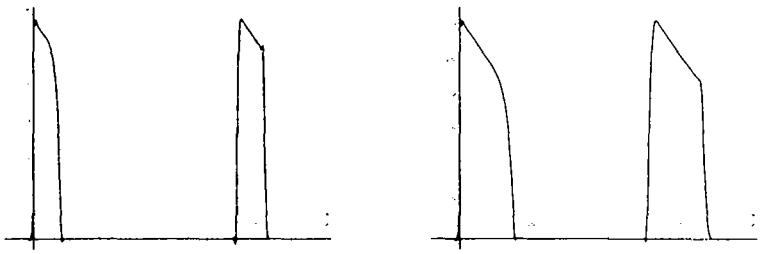

Figure 8: Density of α for uniform noise, measure "max". On the left on each plot: density for plane; on the right: density for step; Left plot: $s_1 = 5$ and $s_2 = 25$ for the step, $s = 5$ for the plane; Right plot: $s_1 = 2.5$ and $s_2 = 12.5$ for the step, $s = 2.5$ for the plane.

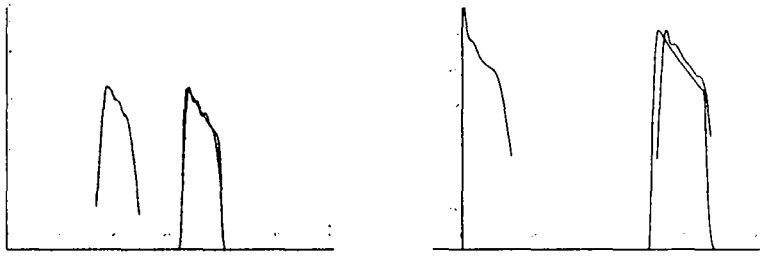

Figure 9: Left: validation for sum measure, uniform noise; Right: validation for max measure, uniform noise.

Simulation process If estimating the mean and variance of a random variable is in general rather quick, estimation of the density is very sensitive to the number of experiments, the discretization of the values taken by the variable. We have adopted a method based on the fundamental theorem of statistics to estimate the density. For each estimation, we performed 40,000 realizations of α, values of f_α are computed on deciles of the repartition function. This is largely enough to estimate properly the range of values taken by α, its mean and variance, but, as the convergence rate of the discrete measure is slow, the density graph is affected by perturbations. In order to obtain a better approximation, we use the repartition function. Figure 9 shows the validation of the method for "sum" and "max" measure with uniform noise. Each of its plots contains on the right the simulated density for a step with $s_1 = 2.5$ and $s_2 = 12.5$ superposed with the theoretical density, and on the left the simulated density for a plane with $s = 2.5$. One can verify that confusion of a singularity with a plane is impossible, and that the simulation process is accurate. Figure 10 shows an experiment on "iso" measure on 5 gray levels. Each plots shows the repartition function for a plane and a step with 2 values of noise. Plan function is the inside one. Left plot corresponds to gaussian noise, middle plot to uniform noise and right plot to Rayleigh noise, Very high blurring has been performed: $s_1 = 2$ and $s_2 = 5$ for gaussian and Rayleigh noise, $s_1 = 1.66$ and $s_2 = 5$ for uniform noise. Despite of this, confusion between plane and step is nearly impossible.

4.2.4 Results

We first present the detection of a step singularity blurred with rayleigh noise. Result is shown on figure 11. We can see that edge detected by a Canny-Deriche filtering is irregular, and edges detected by multifractal exponent are far less sensitive to noise. On figure 12, we can see the detection of a line

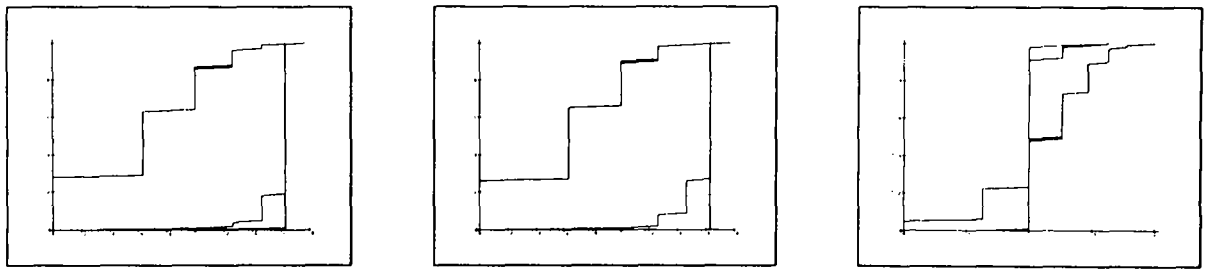

Figure 10: iso measure with gaussian noise (left), uniform noise (middle) and rayleigh noise (right). On each figure, plots represent the repartition function for plane (center) and singularity of type step-edge.

blurred with uniform noise. The line is detected with a fair accuracy by multifractal exponent, and not at all by Canny's filter. We should here have used a specific filter for lines. However, the same multifractal exponent is able to detect both step-edge and line.

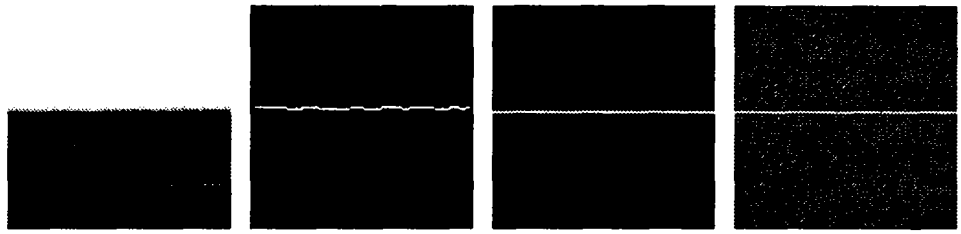

Figure 11: from left to right: blurred step, Canny's edge, edge detected with max measure on $V(3)$, with sum measure on $V(3)$.

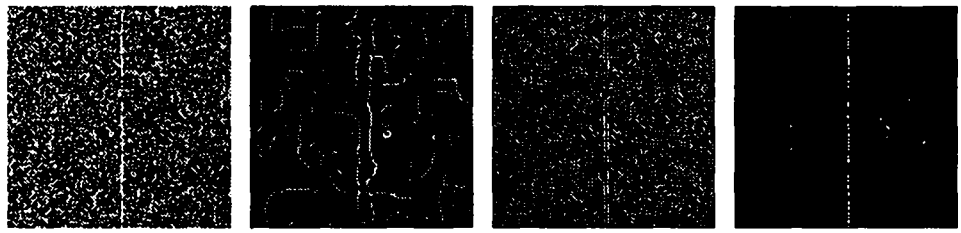

Figure 12: from left to right: blurred line, Canny's edge with large bandwidth, with small bandwidth and edge detected with iso measure, 9 gray levels on $V(3)$.

We then present a compared result on a natural scene (figure 13). We can see on that figure that the multifractal exponent is able to detect small details accurately. The most remarkable is the accuracy of the detection of the corners of the door and of the limits of the bush, when Canny's edges only gives good results in presence of a step.

4.2.5 Use of $f(\alpha)$

In the images presented so far, the use of α computed with well chosen measures has proven to be sufficient. However, this will not always be the case. In this section, we do no more than indicate how the use of $f(\alpha)$ could help us refine our edge detection. Let us consider figure 14.

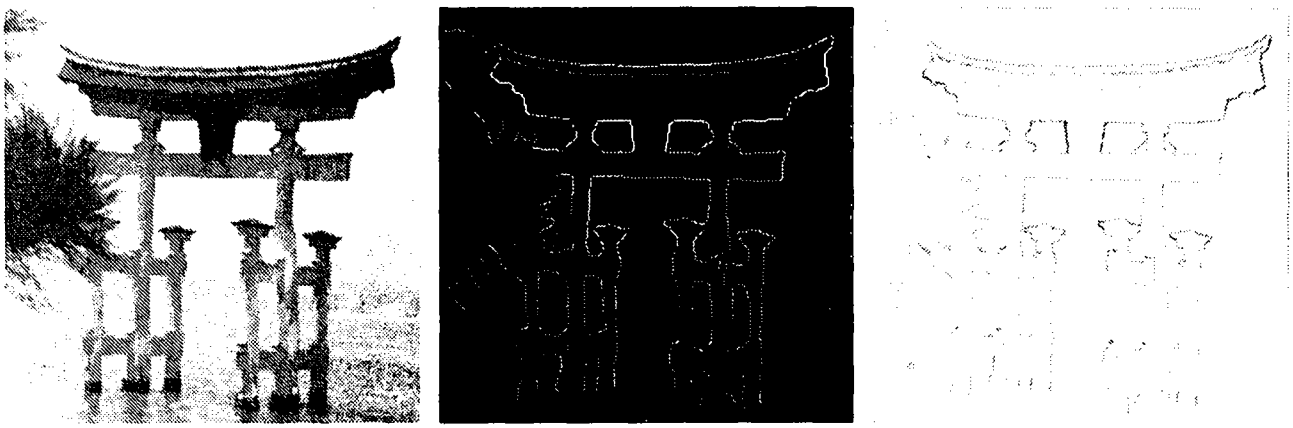

Figure 13: Left: original image, middle: Canny's edges, right: exponent computed with min measure on $V(3)$.

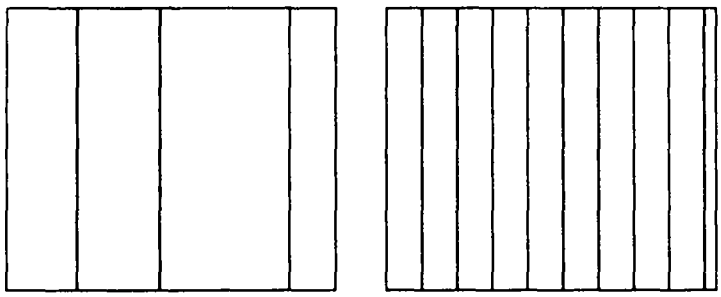

Figure 14: Left: Some edges. Right: A texture.

On the left, anyone would see three edges, that are easily detected by any edge detector. On the right, we have done nothing else than triple the number of lines in the image. Of course, it is still possible to interpret this image as being composed of nine edges, but most people would prefer to talk of a binary texture. However our local computation of exponent α would be the same in both situations.

Here appears another characteristic feature of an edge: an edge does correspond to a certain type of singularity in the images, or to an extremum of the gradient (local characterization), but also to a "rare" event, in some sense that has to be defined. In other words, if too many "edges" are detected in a portion of an image, then the human visual system will have a tendency to talk of a textured zone, rather than of a concentration of edges. In the same way, corner points are even rarer events, and if we group many corner points in a portion of an image (see figure 15), we shall again wish to talk of a texture.

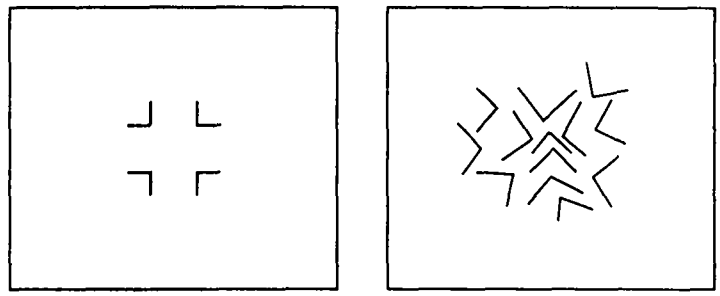

Figure 15: Left: Four corners. Right: A corners' texture.

This is where the $f(\alpha)$ characterization can help us. Remember that $f(\alpha)$ measures, loosely speaking, how rare or frequent an event of singularity α is.

Now we need to say that an edge is characterized both by a given singularity value (local condition) and by the fact that it is in some sense a rare event (global condition). The following procedure can then be used:

- group all points whose α corresponds to the theoretical singularity of an edge: we thus construct the set E_α of section 2,
- compute $f(\alpha)$, the Haussdorff dimension of E_α. If $f(\alpha)$ is equal to one, then we know that the set of selected point "looks" like a set of lines, and does indeed correspond to (regular) contours. If $f(\alpha)$ is slightly greater than one (say for instance 1.2 or 1.3), E_α may correspond to very irregular and jaggy edges. In the case where $f(\alpha)$ is close to 2 (say for instance greater than 1.8), the set E_α contains "too many" points to be considered as a set of edge points. More precisely, if $f(\alpha) = 2$, E_α will be dense in a region of the image, meaning that the singular points fill a part of it, and that they should rather be considered as belonging to a texture. On the contrary, if $f(\alpha)$ is significantly smaller than 1 (say 0.3), it means that we have detected very rare events (a dust of points), that could correspond to corners, or other special points.

To illustrate this, we show in figure 16:

- the points of figure 13 (original image) where $f(\alpha) \approx 1$; one can verify that we get most edge points of the original image.
- the points belonging to the sets E_α (there might be several such E_α sets) such that $f(\alpha) \approx 2$. Here we keep all the points lying inside regions.

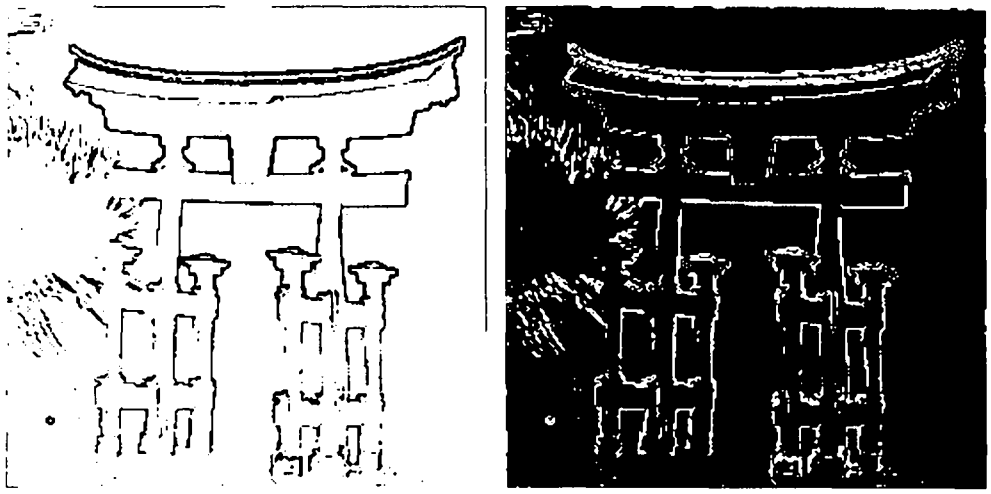

Figure 16: Left: image of points (in white) whose $f(\alpha) = 1.93$. Right: image of points (in white) whose $f(\alpha) = 1.1$.

Much more work is needed in this direction, but these preliminary results show that the $(\alpha, f(\alpha))$ approach might be able to build a bridge between the two so far unconnected methods of edge detection and region extraction.

5 Conclusion

In this work, we have demonstrated that the use of a multifractal characterization of image points can help to solve the problem of edge detection. Our experiments show that, in several cases, this approach gives at least as good results as the classical ones. However, much more work is needed, particularly on the following points:

- precise computation of $f(\alpha)$ on images,
- use of the whole information included in the multifractal spectrum $(\alpha, f(\alpha))$ for a global approach to the problems of edge detection and region extraction.

Acknowledgments

This research has been partially supported by Digital Equipment Corporation.

References

[1] Amar Ait-Kheddache and Sarah A.Rajala. Texture classification based on higher-order fractals. In *IEEE*, 1988.

[2] M. Barnsley and S. Demko. Iterated function system and the global construction of fractals. *Proceedings of the Royal Society*, A 399:243–245, 1985.

[3] M. Barnsley, V. Ervin, D. Hardin, and J. Lancaster. Solution of an inverse problem for fractals and other sets. *Proc. Natl. Acad. Sci. USA*, 83, 1986.

[4] B.Dubuc. *Evaluating the Fractal Dimension of Surfaces*. PhD thesis, McGill University, July 1988.

[5] Benoit B.Mandelbrot. *The Fractal Geometry Of Nature*. W.H.Freeman and company, 1977.

[6] G. Brown, G. Michon, and J. Peyrière. On the multifractal analysis of measures.

[7] J.F. Canny. Finding edges and lines in images. Technical Report TR. 720, MIT Artificial Intelligence Laboratory, June 1983.

[8] R. Deriche. Using canny's criteria to derive a recursively implemented optimal edge detector. *International Journal of Computer Vision*, 1(2), May 1987.

[9] U. Frisch and G.Parisi. *Turbulence and predictability in geophysical fluid dynamics and climate dynamics*, page 84. M. Ghil, R. Benzi and G. Parisi, Amsterdam (Holland), 1895.

[10] H.G.E Hentschel and I.Procaccia. The infinite number of generalized dimensions of fractals and strange attractors. *Physica 8D*, 1983.

[11] I.Procaccia. The characterization of fractal measures as interwoven sets of singularities : Global universality at the transition to chaos. Technical report, Department of Chemical Physics, The Weizmann Institute of Science, Rehovot 76100, Israel, 1986.

[12] S. Jaffard. Construction de fonctions multifractales ayant un spectre de singularités prescrit. *C.R. Acad. Sci. Paris*, pages 19–24, 1992. T. 315, Série I.

[13] B. Kahng. Negative moments of current distribution in random resistor networks. *Physical Review Letters*, 64:914–917, 1990.

[14] James M. Keller, Susan Chen, and Richard M. Crownover. Texture description and segmentation through fractal geometry. *Computer Graphics and Image Processing*, 45:150–166, 1989. Edited by Academic Press.

[15] J. Lévy Véhel. About lacunarity, some links between fractal and integral geometry, and an application to texture segmentation. In *ICCV*, 1990.

[16] J. Lévy Véhel. Fractal probability functions : an application to image analysis. In *CVPR*, 1991.

[17] J. Lévy Véhel, P. Mignot, and J.-P. Berroir. Multifractal, texture, and image analysis. In *Proc. International Conference on Computer Vision and Pattern Recognition*, 1992. Maui.

[18] J. Lévy Véhel, P. Mignot, and J.P. Berroir. Multifractals, texture, and image analysis. In *CVPR*, 1992.

[19] S. Lovejoy, A. Davis, P. Gabriel, Schertzer D., and G. Austin. Discrete angle radiative transfer. 1. scaling and similarity, universality and diffusion. *Journal of Geophysical Research*, 95:699–715, 1990.

[20] B.B Mandelbrot. *The Fractal Geometry of Nature*. CA: Freeman, San Fransisco, 1982.

[21] B.B. Mandelbrot. A class of multinomial multifractal measures with negative (latent) values for the dimension $f(\alpha)$. In *Fractals (Proceedings of the Erice meeting)*. L.Pietronero, New York, 1989.

[22] B.B. Mandelbrot. Fractal measures (their infinite moment sequences and dimensions) and multiplicative chaos: Early works and open problems. Technical report, Physics Department, IBM Research Center, Mathematics Deparment, Harvard University, Cambridge, MA 02138, USA, 1989.

[23] O. Monga. An optimal region growing algorithm for image segmentation. *International Journal of Pattern Recognition and Artificial Intelligence*, 1(3), December 1987. Paris, France.

[24] O. Monga and R. Deriche. 3d edge detection using recursive filtering. In *Conference on Vision and Pattern Recognition*, San-Diego, USA, June 1989. IEEE.

[25] Y. Oono. Large deviation and statistical physics. *Progress of Theoritical Physics Supplement*, 99:165–205, 1989.

[26] S. Peleg, J. Naor, R. Hartley, and D. Avnir. Multiple resolution texture analysis and classification. *IEEE*, PAMI-6(4), July 1984.

[27] A. Pentland. Fractal-based description of natural scenes. *IEEE*, PAMI-6, 1984.

[28] T.C. Hasley M.H. Jensen L.P. Kadanoff I. Procaccia B.I. Shraiman. Fractal measures and their singularities: The characterization of strange sets. *Physical Review*, February 1986.

Unité de Recherche INRIA Rocquencourt
Domaine de Voluceau - Rocquencourt - B.P. 105 - 78153 LE CHESNAY Cedex (France)

Unité de Recherche INRIA Lorraine Technopôle de Nancy-Brabois - Campus Scientifique
615, rue du Jardin Botanique - B.P. 101 - 54602 VILLERS LES NANCY Cedex (France)
Unité de Recherche INRIA Rennes IRISA, Campus Universitaire de Beaulieu 35042 RENNES Cedex (France)
Unité de Recherche INRIA Rhône-Alpes 46, avenue Félix Viallet - 38031 GRENOBLE Cedex (France)
Unité de Recherche INRIA Sophia Antipolis 2004, route des Lucioles - B.P. 93 - 06902 SOPHIA ANTIPOLIS Cedex (France)

EDITEUR
INRIA - Domaine de Voluceau - Rocquencourt - B.P. 105 - 78153 LE CHESNAY Cedex (France)

ISSN 0249 - 6399